Title
Measurement of High-Energy Neutron Flux Above Ground Utilizing a Spallation Based Multiplicity Technique

Journal
IEEE Transactions on Nuclear Science, 63(6)

ISSN
0018-9499

Authors
Roecker, Caleb
Bernstein, Adam
Marleau, Peter
et al.

Publication Date
2016-12-01

DOI
10.1109/tns.2016.2628644

Peer reviewed

Measurement of High-Energy Neutron Flux Above Ground Utilizing a Spallation Based Multiplicity Technique

Caleb Roecker, *Student Member, IEEE*, Adam Bernstein, Peter Marleau, *Member, IEEE*, and Kai Vetter, *Member, IEEE*

***Abstract*— Cosmogenic high-energy neutrons are a ubiquitous, difficult to shield, poorly measured background. Above ground the high-energy neutron energy-dependent flux has been measured, with significantly varying results. Below ground, high-energy neutron fluxes are largely unmeasured. Here we present a reconstruction algorithm to unfold the incident neutron energy-dependent flux measured using the Multiplicity and Recoil Spectrometer (MARS), simulated test cases to verify the algorithm, and provide a new measurement of the above ground high-energy neutron energy-dependent flux with a detailed systematic uncertainty analysis. Uncertainty estimates are provided based upon the measurement statistics, the incident angular distribution, the surrounding environment of the Monte Carlo model, and the MARS triggering efficiency. Quantified systematic uncertainty is dominated by the assumed incident neutron angular distribution and surrounding environment of the Monte Carlo model. The energy-dependent neutron flux between 90 MeV and 400 MeV is reported. Between 90 MeV and 250 MeV the MARS results are comparable to previous Bonner sphere measurements. Over the total energy regime measured, the MARS result are located within the span of previous measurements. These results demonstrate the feasibility of future below ground measurements with MARS.**

***Index Terms*— Cosmogenic neutrons, high-energy neutron spectroscopy.**

I. Introduction

SECONDARY particles arising from cosmogenic high-energy neutrons form a ubiquitous and prominent background in a wide range of particle and nuclear physics experiments. Examples of high-energy neutron induced backgrounds include: the generation of secondary radiation which may impact gamma ray and neutron based measurements [1]–[3] and indirect backgrounds for many rare-event neutral particle experiments (e.g. antineutrino reactor monitors [4], WIMP dark matter detectors [5], neutrinoless double beta decay detectors [6], and coherent neutrino nucleus scattering detectors [7]).

The energy-dependent flux of these cosmogenic neutrons has been measured by several groups above ground, but is largely unmeasured below ground. Above ground high-energy neutron measurements have been summarized by Ziegler (Fig. 18 of [1]) and show significant disagreement. Significant uncertainty exists in these measurements due primarily to three factors: an unknown and probably energy dependent neutron angular distribution [1], individual detector systematic biases, and a lack of an active charged particle veto in many of the previous experiments [8], [9].

In order to measure the high-energy neutron energy-dependent flux we have constructed the Multiplicity And Recoil Spectrometer (MARS). A detailed description of the system and the signatures that it measures are described in [10]. MARS consists of two large Gd containing plastic scintillator detectors surrounding a large number of lead bricks. Incident high energy neutrons induce spallation reactions in the lead producing many secondary neutrons of significantly lower energy. These secondary neutrons thermalize in the scintillator and are captured by a Gd nucleus resulting in an 8 MeV cascade of gamma rays. MARS records the deposited energy of the secondary neutrons during the thermalization process (thermalization energy), the number of Gd captures (multiplicity), and the energy deposited by all Gd captures (capture energy). MARS is not capable of directly measuring the high-energy neutron flux angular distribution. However, our analysis includes the incident angular distribution as a systematic uncertainty. Additionally, MARS includes an active charged particle veto and it uses a different reconstruction analysis than previous above ground measurements.

The primary purpose of this paper is to provide a new measurement of the high-energy neutron energy-dependent flux above ground using the MARS detector. Our results demonstrate the feasibility of future MARS measurements by being located within the spread of previous above ground measurements. Measurements at several underground depths

Manuscript received July 15, 2016; revised September 15, 2016 and October 23, 2016; accepted November 5, 2016. Date of publication November 14, 2016; date of current version December 14, 2016. This material is based upon work supported by the Department of Energy National Nuclear Security Administration under Award Number: DE-NA0000979 through the Nuclear Science and Security Consortium. This work was performed under the auspices of the U.S. Department of Energy by Lawrence Livermore National Laboratory under contract DE-AC5-07NA27344.LLNL-JRNL-695883. Sandia National Laboratories is a multi-program laboratory managed and operated by Sandia Corporation, a wholly owned subsidiary of Lockheed Martin Corporation, for the U.S. Department of Energy's National Nuclear Security Administration under contract DE-AC04-94AL85000. Approved for unlimited release, SAND2016-6353.

C. Roecker is with the Department of Nuclear Engineering, University of California, Berkeley, Berkeley, CA 94720 USA (e-mail: calebroecker@berkeley.edu).

A. Bernstein is with Nuclear and Chemical Sciences Division, Lawrence Livermore National Laboratory, Livermore, CA 94550 USA.

P. Marleau is with Radiation and Nuclear Detection Systems, Sandia National Laboratories, Livermore, CA 94550 USA.

K. Vetter is with Nuclear Science Division, Lawrence Berkeley National Laboratory, Berkeley, CA 94720 USA.

Color versions of one or more of the figures in this paper are available online at http://ieeexplore.ieee.org.

Digital Object Identifier 10.1109/TNS.2016.2628644

were also made and results will be reported in a future paper. In Sec. II the Markov Chain Monte Carlo (MCMC) algorithm implemented to infer the incident neutron energy-dependent flux is briefly described. In Sec. III a simulation test case is unfolded to verify the MCMC algorithm for MARS. In Sec. IV sources of systematic uncertainty are described. In Sec. IV the experimental data and several background estimates are described. Finally Sec. VI presents the measured energy-dependent flux above ground which is compared to the previous measurements of Gordon [11] and to multiple measurements summarized by Ziegler [1].

II. Reconstruction Method

The high-energy neutron energy-dependent flux is reconstructed using an MCMC algorithm. The MCMC algorithm determines the energy-dependent flux of incident neutrons given the measured secondary neutron data and a simulated detector response matrix that is estimated using a Geant4 [12], [13] model of the detector [10].

The algorithm used here was derived by Kuusela [14]. This algorithm is attractive over other reconstruction algorithms due to its ability to calculate reconstruction uncertainty, incorporate a priori information, and minimize the a priori induced bias. In addition, the algorithm uses cubic basis splines, defined by a set of knots, in order to produce a second order continuously differentiable result [15]. Due to our implementation being nearly identical to the original form of the algorithm, we direct the reader to the paper by Kuusela [14]. The only change we made was to include a background term. Here, we only provide the necessary equations to set up the problem.

To solve for the incident neutron energy-dependent flux, the inverse algorithm must solve the Fredholm integral equation

$$g(\vec{y}) = \int A(E, \vec{y}) f(E) dE + b(\vec{y}), \tag{1}$$

where $g(\vec{y})$ is the measured secondary neutron response, $A(E, \vec{y})$ is the detector response matrix estimated using Monte Carlo simulation, $f(E)$ is the desired energy-dependent flux, $b(\vec{y})$ is the background due primarily to the ambient gamma ray flux, $\vec{y}$ is the vector of measured parameters, and E is the incident neutron energy. Because the continuous form of the parameters are not known, Eq. 1 must be discretized:

$$\vec{g}_{meas} = \mathbf{A}\vec{f} + \vec{b}, \tag{2}$$

where $\vec{g}_{meas}$ is a vector of length N, $\mathbf{A}$ is a N by P matrix, $\vec{f}$ is a vector of length P, and $\vec{b}$ is a vector of length N. The energy-dependent flux is discretized in the following manner:

$$f(E) = \sum_{i=1}^{P} \vec{f}_i \beta_i(E), \tag{3}$$

where $\beta_i(E)$ is the i-th cubic basis spline function and $\vec{f}_i$ is the i-th basis spline coefficient. In the context of the above discretization, N is the number of voxels in the measured vector ($\sim$1700) and P is the number of basis spline coefficients (8).

For MARS, $\mathbf{A}$ is not square eliminating the possibility of direct matrix inversion of Eq. 2. Pseudo-matrix inversion, using a Moore-Penrose matrix [16], of Eq. 2 is not advisable given the rank deficient nature of $\mathbf{A}$ and the background in Eq. 2 [17]. The problem is ill-posed; to solve for $f(E)$ the algorithm uses a Bayesian approach with regularization:

$$p(\vec{f}|\vec{g}_{meas}, \vec{b}, \alpha) = \frac{p(\vec{g}_{meas}, \vec{b}|\vec{f}) p(\vec{f}|\alpha)}{p(\vec{g}_{meas}, \vec{b}|\alpha)}, \tag{4}$$

where α is the regularization strength, $p(\vec{f}|\vec{g}_{meas}, \vec{b}, \alpha)$ is the Bayesian posterior, $p(\vec{g}_{meas}, \vec{b}|\vec{f})$ is the likelihood given the Poisson statistics of the problem, $p(\vec{f}|\alpha)$ is the regularization prior, and $p(\vec{g}_{meas}, \vec{b}|\alpha)$ is the marginal likelihood. The likelihood for Poisson statistics is defined by:

$$p(\vec{g}_{meas}, \vec{b}|\vec{f}) = \prod_{i=1}^{N} \left(e^{-\left((\mathbf{A}\vec{f})_i + \vec{b}\right)} \right) \frac{\left((\mathbf{A}\vec{f})_i + \vec{b}\right)^{\vec{g}_{meas,i}}}{(\vec{g}_{meas,i})!}, \tag{5}$$

where i is the vector element, $\mathbf{A}\vec{f}$ is the forward projected answer, and all other parameters have been previously defined. We use a curvature regularization defined by:

$$p(\vec{f}|\alpha) \propto exp\left(-\alpha \int (f''(E))^2 dE\right) = exp(-\alpha \vec{f}^T \Omega \vec{f}), \tag{6}$$

where Ω is the curvature matrix. In the cubic basis spline parameterization the curvature matrix Ω is defined by:

$$\Omega_{i,j} = \int \beta_i''(E) \beta_j''(E) dE, \tag{7}$$

where $\beta_i''(E)$ is the second derivative of the i-th cubic basis spline. The marginal likelihood is handled by the MCMC algorithm and is not formally defined.

We employ Aristotelian boundary conditions by adding a positive constants to $\Omega_{1,1}$ and $\Omega_{P,P}$ [14], [18]. For simplicity we use the same constant and fix it to $\Omega_{1,1}$. The regularization matrix Ω is positive definite. With the above definitions we can perform the algorithm described by Kuusela [14] to solve for the optimal regularization strength α. With an optimal α, a boot-strapping procedure [14], [19] can be used to reduce the bias introduced by the regularization resulting in $f(E)_{BC}$, the bias corrected reconstruction. In the context of the MARS measurement, boot-strapping is performed by Poisson sampling the forward projected vector $\mathbf{A}\vec{f}$ and the background vector $\vec{b}$ and combining them to replace $\vec{g}_{meas}$. Here the bootstrapping procedure is performed ten times per iteration and five iterations are used. We observe minimal change in $f(E)_{BC}$ after five bias corrections indicating that the bias reduction converged. After removing the bias an additional 2000 bootstrap samples are drawn at the recommendation of Efron and Tibshirani [19]. The set of the final bias corrected samples, $F = \{f(E)^r_{BC}\}_{r=1}^{2000}$, from the bootstrapping procedure can be used to construct confidence intervals. We calculate confidence intervals by using the bootstrap percentile intervals. The set of functions F are evaluated at E in increments of 1 MeV to find the x and $1-x$ percent evaluations at each E. Intervals are constructed by:

$$[f(E)_{BC,x}, f(E)_{BC,1-x}] \tag{8}$$

where $f(E)_{BC,x}$ is x percent function evaluation at E.

III. Simulation Results

To investigate whether the reconstruction algorithm briefly described in Sec. II produces correctly reconstructed results, we used the MARS Monte Carlo model described in [10] to simulate 5 groups of neutrons at energies of 100, 200, 300, 500, and 700 MeV. Neutrons were generated on the upper half sphere surface of the model in a cosine distribution. The detector response was applied to the deposited simulated energy given the ADC timing parameters described in [10].

Using the definition for depositions and events described in Sec. I of [10] and the event identification algorithm described in Sec. 5 of [10], neutron multiplicity events are classified as:

1) All individual depositions must have $\geq$ 850 keV deposited energy
2) The start of the event must occur $>$ 200 μs from a veto deposition
3) An event is recorded if $\geq$ 3 depositions occur within 25 μs
4) Additional depositions can be added to an event if they occur $\leq$ 75 μs from the second to last deposition already recorded in an event
5) Only the first deposition may be over 8 MeV
6) An event with multiplicity 3 must have $(Capture\ Energy[MeV])/Multiplicity > 2.0\ MeV$

The MARS Monte Carlo model was used to simulate incident neutrons until 100,000 multiplicity events were recorded for each incident neutron energy. The capture energy was binned in 8 MeV increments. The thermalization energy was binned given an energy resolution 30% worse than determined in Sec. 4 of [10] with the caveat that each bin must be $\geq$ 8 MeV in width. This coarse energy binning in the thermalization and capture energy ensures that energy calibration or gain correction measurements do not dominate the systematic uncertainty.

The MCMC algorithm was used to reconstruct the input neutron counts. The distribution of reconstructed and input counts in the cubic basis spline space is observed in Fig. 1. The output energy knot spacing for each of the 5 simulated energies was fine near the respective energy and became more coarse at a greater distances from the mono-energetic peak. The binning was adjusted in order that multiple $\vec{f}_i$ had Gaussian distributions and no oscillations were observed in the reconstructed output.

Examining Fig. 1, we observe a broadening of the reconstructed energy indicating the degradation of the energy resolution. Additionally some reconstruction means have a slight offset from the input energy. In these situations, the peak reconstructed value is offset by one basis spline from the correct position. This offset is not considered problematic because Fig. 1 has a finer knot spacing than is used in an experimental analysis. Coarser spacing of the basis spline knots reduces the probability of offset. In spite of the offset, we observe consistent predictions of the number of simulated incident neutrons which are displayed in Table I. In Table I, the input column displays the number of incident neutrons simulated. Of these simulated incident neutrons, 100,000 neutrons initiated events passing the MARS event requirements.

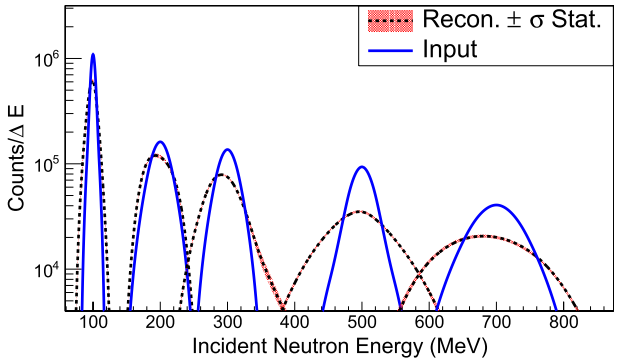

Fig. 1. The reconstructed counts/ΔE of the 5 mono-energetic neutron simulations. The input spectra in the cubic basis spline space is displayed as a solid blue line. Reconstructed spectra are displayed as a dashed black line. Confidence intervals around the reconstructed spectra are displayed as a patterned red area.

TABLE I

The Integral Number of Neutrons Simulated for the 5 Mono-Energetic Neutron Energies. The Input, Bias Corrected Reconstruction, and the Integral of the $\pm 1\sigma$ Confidence Interval Functions Are Displayed

Energy (MeV)	Input 10^6	$f(E)^{+\sigma}_{-\sigma}$ 10^6
100	10.6	$10.9^{+0.4}_{-0.4}$
200	6.47	$6.60^{+0.2}_{-0.2}$
300	5.46	$5.55^{+0.2}_{-0.2}$
500	4.55	$4.59^{+0.2}_{-0.1}$
700	4.06	$4.11^{+0.2}_{-0.2}$

The $f(E)$ column reports the predicted number of simulated events and includes 1-σ uncertainty estimates. The quoted uncertainty in Table I only includes statistical considerations.

IV. Systematic Uncertainty Considerations

Sources of systematic uncertainty for the MARS experimental analysis include: the unknown incident neutron angular distribution, the surrounding environment considered by the Monte Carlo model, the secondary neutron capture efficiency, the multiplicity event triggering efficiency, and the uncertainty in the gain drift and energy calibration. The uncertainty associated with the gain drift and energy calibration is minimized by design of the measured data. The coarse energy binning of the thermalization and capture energy described in Sec. III make it unlikely that gain shifts or systematic bias in the position dependent energy calibration will cause shifts in the recorded data.

The secondary neutron capture characteristics for MARS were well characterized using a Cf-252 source in [10]. We observed excellent agreement between the neutron capture efficiency and reasonable agreement with the neutron capture time. The slight discrepancy in the capture time produces a small deviation in the MARS event tagging efficiency. The triggering analysis described in Sec. III used an initial time range of 25 μs with a possible expansion of 75 μs from the second to last deposition. To characterize the uncertainty in

the event tagging efficiency, we vary the initial time range from 22μs to 28μs. The secondary time range was left fixed at 75μs. The variation in the initial time range is based upon the ratio of the initial time range and the capture time:

$$\frac{25\mu s}{t_{sim}} \approx \frac{25\mu s + x\mu s}{t_{exp}}, \tag{9}$$

where t_{sim} is the capture time from the simulation, t_{exp} is the capture time from the measured data [10], and x is the variation. We conservatively round x up to 3 μs, and assume the variation is symmetric ($\pm$ 3 μs). We found the systematic uncertainty due to the event identification to be relatively small when compared to other systematic uncertainties.

Two Monte Carlo models were used to simulate the MARS detector and its environment. The first was the partial geometry model, including only the detectors, lead, steel table, and associated vetoes. The second was the full geometry model, including the detectors, lead, steel table, associated vetoes, deployment platform, and several meters of rock underneath the deployment platform. We use rock in order to use the same model for the below ground measurements. The minimal amount of topsoil present above ground at the Kimballton Underground Research Facility (KURF) is assumed to have a small impact on the results. We found that the variation of the MARS results as a function of the surrounding environmental model was on the same order as the incident angular distribution (Sec. VI). However we do not have a multitude of environmental models to compare, making it difficult to calculate a systematic uncertainty. We therefore average these distributions using a convolution and use each individual distribution to construct the systematic uncertainties.

Finally the incident neutron angular distribution is of particular concern since MARS has no direct method of measuring the angular distribution. Instead a reasonable range of possible angular distributions has been investigated. Typically the incident neutron angular distribution is characterized as $\propto cos^n(\theta)$, where θ is the angle relative to the zenith [1]. Ziegler summarizes several works which attempt to calculate the angular distribution. Using the data summarized by Ziegler: [20]–[24] except for Lohrmann et al. [25] and the newly processed data from Moser et al. [26], we calculate a mean angular distribution of $\cos^{3.0\pm0.6}(\theta)$. Several of the experiments referenced by Ziegler indicate that the angular distribution is probably dependent upon the incident neutron energy. However, we do not consider this variation since no robust measurements of the energy dependence have been performed. Examining the effective area calculations of MARS [10], we observe that as the power of cosine increases, the change in effective area decreases. The largest increase in the effective area occurs at low integer powers of $\cos^n(\theta)$. Additionally we observe minimal change in the reconstructed neutron energy-dependent flux with incident angular distributions steeper than $\cos^4(\theta)$. Here, we report the above ground reconstructed neutron energy-dependent flux assuming $\cos^3(\theta)$. Incident angular distributions of $\cos^2(\theta)$ and $\cos^4(\theta)$ are used in the systematic uncertainty analysis. We consider this a conservative estimate of the systematic variation of the incident angular distribution.

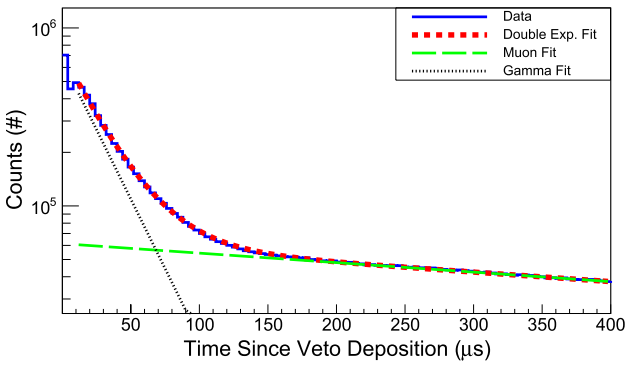

Fig. 2. The neutron detector deposition time after a tagged muon veto deposition. The signal is composed of two exponential distributions. The exponential with the faster time constant is due to muon induced depositions in the detector. The long time constant exponential is due to the uncorrelated gamma-ray flux.

V. Experimental Data and Background Predictions

MARS operated at the surface of earth above KURF at an atmospheric depth of 1029.76 g/cm^3 (500 m above sea level) near 37-23-00.4 North, 080-39-29.2 West. The location is near the entrance to the mine where KURF is located and is distantly surrounded by large hills. MARS was situated several meters from an out-building composed of cinder blocks. The closest surface to the detector remained the soil underneath the deployment platform. The measurement was performed starting on April 24th, 2015 and operated for 9 days with a live-time of 7 days. A combined neutron detector count rate of 3 kcps was observed.

To remove multiplicity events due to muon-induced spallation, a 200μs veto time was used. An effective veto time was determined by investigating the neutron detector deposition time after a muon was tagged by the veto paddles and the neutron detectors. As observed in Fig. 2 after $\sim$5μs the distribution is a summation of two exponential distributions, corresponding to a sharply decreasing muon-induced distribution and a longer uncorrelated gamma-ray induced distribution. By using a 200μs veto time we eliminate a majority of the muon-induced signal. This 200μs veto time is initiated after every veto deposition. The veto energy threshold was set at 2 MeV for all paddles in order to remove nearly 100% of the muon induced multiplicity signal. Due to the low energy threshold of the veto paddles, most veto depositions are due to uncorrelated gamma rays resulting in 19% dead time. While this dead time might be considered high for some applications, it is not reducible given the desire for a clean neutron multiplicity signal. After the veto rejection and the event requirements applied from Sec. III, MARS observed $\sim$2.9 million neutron like events.

A simple Monte Carlo model based upon the measured uncorrelated gamma ray background rate and the individual multiplicity event gate length was used to estimate the gamma ray contamination of the multiplicity data. Using this model, we determine that 9% of neutron like events were partially contaminated by gamma rays. Nearly all of this contamination is due to a single gamma ray contaminating neutron

multiplicity events. Contamination of a multiplicity event by multiple gamma rays was predicted to be less than 0.5%.

The charged particle contamination was simulated using the CRY package [27] with all particles except neutrons. The simulation was run with the partial geometry model which only included the detector and the veto system: the surrounding environment was not modeled. The detector position dependent response, the experimental energy threshold, and the event requirements described in Sec. III were applied to the simulated data. We predict 970± 15 contamination events corresponding to 0.03% of the measured event number. Due to this insignificant percentage we do not consider charged particle contamination above ground., Subtracting the background from the measured data is not straightforward. The difference between two Poisson distributions is not a Poisson distribution. This problem requires that a background subtraction be performed inside the boot-strapping procedure. While 2000 bootstrap samples was suggested as a sufficient number by Efron and Tibshirani [19] for calculating confidence intervals, no guidance is provided given the additional bootstrap of the background subtraction. The mean value of the reconstruction does shift between background subtracted and non-background subtracted data. However, we observe insignificant differences between the background subtracted and non-background subtracted reconstructions with regard to the percent difference of the confidence intervals.

VI. Experimental Results

Using the reconstruction of the mono-energetic neutron simulations in Sec. III, a minimum knot spacing as a function of energy can be calculated for the final experiment results $f(E)_{BC}$. We used this minimum knot spacing as a starting point and increased various knot distances until the reconstruction result did not shift with small perturbations to the knot positions. All results are scaled using the method of Gordon [11] to correct for geomagnetic rigidity and elevation.

We consider the best model to be the average by convolution of the full and partial geometry model with an incident angular distribution of $\cos^3(\theta)$. Angular distributions of $\cos^2(\theta)$ and $\cos^4(\theta)$ are used to estimate the systematic uncertainty. The percent difference between $\cos^3(\theta)$ and various permutations of the angular distribution using the average of both Monte Carlo models without uncertainty are shown in Fig. 3. The percent difference between the average of both Monte Carlo models and each respective Monte Carlo model is shown in Fig. 4 without uncertainty. The percent difference between the gating structure of 22μs and 28μs, with the standard 25μs, is shown in Fig. 5 without uncertainty. We observe a maximum percent deviation of 12%. Final results with uncertainty are displayed and compared to the results from Gordon [11] and multiple experiments summarized by Ziegler [1] in Fig. 6. The variance in Fig. 6 is the sum in quadrature of all systematic uncertainties and the statistical uncertainty as a function of energy in 1 MeV increments.

The above ground results in Fig. 6 are comparable with the results of Gordon et al. [11] and Hess et al. [8], [9] between 90 MeV and 250 MeV. Below 90 MeV the result is

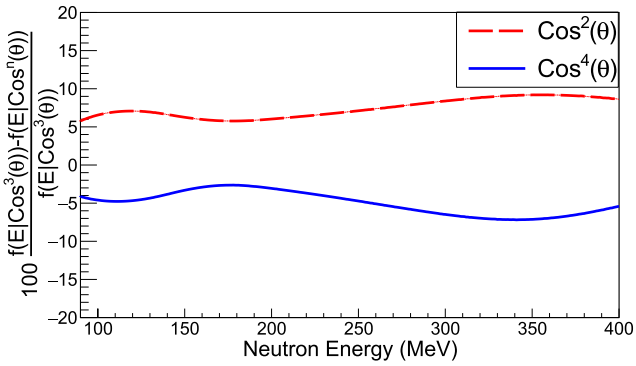

Fig. 3. The percent difference in the reconstructed neutron flux versus energy, between the preferred ($\cos^3(\theta)$) and alternative choices of the neutron angular distribution. The partial geometry model was used for this comparison.

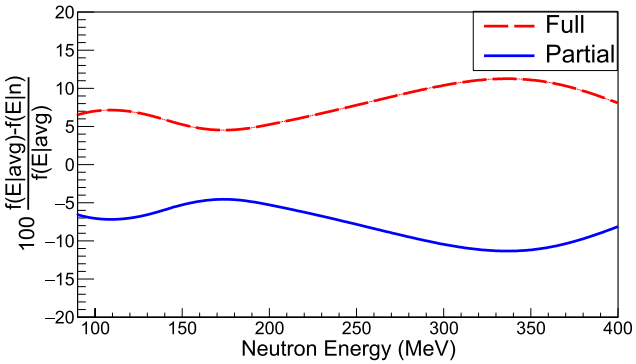

Fig. 4. The above ground reconstructed neutron energy-dependent flux at KURF for the partial and full geometry models given an incident angular distribution of $\cos^3(\theta)$.

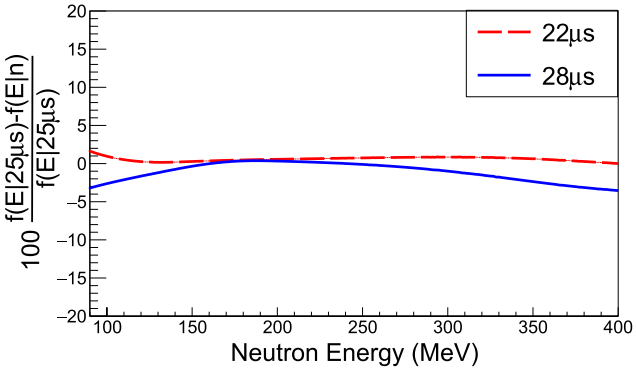

Fig. 5. The above ground reconstructed neutron energy-dependent flux at KURF with variation in the initial gate triggering time given an incident angular distribution of $\cos^3(\theta)$.

constrained by the detector efficiency and boundary conditions employed by the reconstruction analysis. Above 250 MeV, we measured a slightly lower flux than most previous experiments. Regardless of the energy regime, our results are contained within the spread of previous measurements. Where available, our total uncertainties are comparable to total uncertainty of other experiments.

We are uncertain whether the deviation above 250 MeV is due to other experiments lacking an active charged particle veto or the uncertainty in the incident neutron angular distribution. The deviation may also be due to Ziegler summarizing

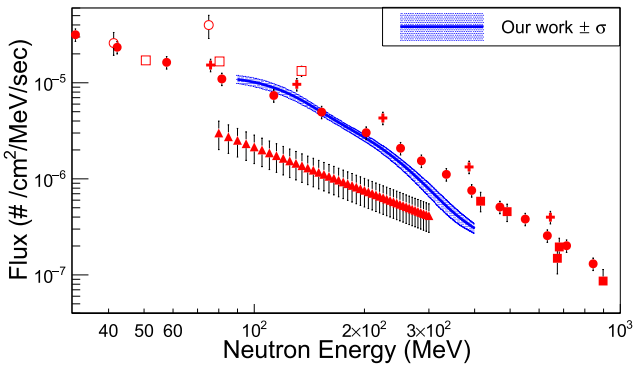

Fig. 6. The above ground reconstructed neutron energy-dependent flux at KURF compared to previous experiments. The previous experimental data correspond to the following shapes: Ashton et al. ■ [28], Gordon et al. ✚ [11], Heidbreder et al. ▲ [22], Hess et al. ● [8], [9], Preszler et al. ○ [29], and R. Saxena □ [24]. The results from Ashton [28] were scaled by Ziegler [1] due to the unknown incident angular distribution.

the total hadron flux and assuming it is dominated by the neutron component. Ziegler estimates that the hadron flux is 90% neutrons at 100 MeV, but may be 50% protons by 1 GeV. These protons would be actively vetoed from the MARS data. Additionally it seems that the data by Ashton [28] was scaled to match the Hughes corrected Hess data [8], [9]. This inherently biases the Ashton result [28] towards the Bonner sphere measurements. Therefore above 300 MeV, all results are scaled to or performed by Bonner sphere arrays or arrays using a similar principle. The experiment of Heidbreder [22], which forms the lower bound of the previous measurements, was statically limited. No experiment referenced here has inferred the neutron flux using multiple Monte Carlo packages. Finally, no experiment calculates the systematic uncertainty due to the varying magnetic strength of the heliosphere.

The MARS measurement could exhibit environmental variation due a large hill on one side of the detector which could decrease the high-energy neutron flux. However, we expect this variation to be significantly less than the difference between the full and partial geometry models. Additionally, no systematic uncertainty analysis of the Geant4 neutron lead spallation model was performed, either through measurement or by using different Geant4 physics lists. Measuring the bias and uncertainty associated with the Geant4 neutron lead spallation models, with MARS at an accelerator facility, would be difficult given the long triggering time of MARS to record an event (100's of μs). In the absence of measuring this bias or uncertainty, we used the Geant4 Shielding physics list which is recommended for high-energy physics. If future measurements are performed measuring the direct neutron lead spallation reaction, improvements could be made to our results as well as the Bonner sphere results.

VII. Conclusions

We have presented a new above ground measurement of the neutron energy-dependent flux between 90 and 400 MeV utilizing the recently developed MARS spectrometer. This measurement demonstrates the feasibility of the MARS detector and analysis to measure these high-energy neutrons and provides confidence that future and more challenging below ground measurements with MARS will reconstruct an appropriate energy-dependent flux.

MARS operated at earth's surface for a live-time of ~7 days and recorded 2.9 million events with a 19% dead-time. Using an MCMC inversion algorithm, this data was used to reconstruct the incident neutron energy-dependent flux above ground. Between 90 MeV and 250 MeV our results are comparable with previous Bonner sphere measurements. Above 250 MeV our results indicate a slightly lower flux. We predict minimal background contamination in the above ground measured data from charged particles. Predictions of the ambient uncorrelated gamma ray flux are incorporated into a background subtraction within the bootstrap of the reconstruction algorithm. Uncertainty estimates are provided based upon the measurement statistics, the incident angular distribution, the surrounding environment of the Monte Carlo model, and the MARS triggering efficiency. Quantified systematic uncertainty is dominated by the assumed incident neutron angular distribution and surrounding environment of the Monte Carlo model.

References

[1] J. F. Ziegler, "Terrestrial cosmic rays," *IBM J. Res. Develop.*, vol. 40, no. 1, pp. 19–39, Jan. 1996.
[2] J. Kiener *et al.*, "Fast-neutron induced background in $LaBr_3$:Ce detectors," *Nucl. Instrum. Methods, Phys. Res. A*, vol. 798, pp. 152–161, Oct. 2015.
[3] R. T. Kouzes *et al.*, "Cosmic-ray-induced ship-effect neutron measurements and implications for cargo scanning at borders," *Nucl. Instrum. Methods, Phys. Res. A*, vol. 587, no. 1, pp. 89–100, 2008.
[4] A. Bernstein *et al.*, "Nuclear security applications of antineutrino detectors: Current capabilities and future prospects," *Sci. Global Secur.*, vol. 18, no. 3, pp. 127–192, 2010.
[5] M. J. Carson *et al.*, "Neutron background in large-scale xenon detectors for dark matter searches," *Astroparticle Phys.*, vol. 21, no. 6, pp. 667–687, 2004.
[6] M. S. Boswell *et al.*, "Neutron inelastic scattering in natural Cu as a background in neutrinoless double-SS decay experiments," *Phys. Rev. C*, vol. 87, no. 6, p. 064607, 2013.
[7] Collar, *Nucl. Instrum. Methods, Phys. Res. A*, vol. 773, p. 56, 2014.
[8] W. N. Hess, H. W. Patterson, R. Wallace, and E. L. Chupp, "Cosmic-ray neutron energy spectrum," *Phys. Rev.*, vol. 116, pp. 445–457, Oct. 1959.
[9] E. B. Hughes and P. L. Marsden, "Response of a standard IGY neutron monitor," *J. Geophys. Res.*, vol. 71, no. 5, pp. 1435–1444, 1966.
[10] C. Roecker *et al.*, "Design of a transportable high efficiency fast neutron spectrometer," *Nucl. Instrum. Methods, Phys. Res. A*, vol. 826, pp. 21–30, Aug. 2016.
[11] M. S. Gordon *et al.*, "Measurement of the flux and energy spectrum of cosmic-ray induced neutrons on the ground," *IEEE Trans. Nucl. Sci.*, vol. 51, no. 6, pp. 3427–3434, Dec. 2004.
[12] S. Agostinelli *et al.*, "Geant4—A simulation toolkit," *Nucl. Instrum. Methods, Phys. Res. A*, vol. 506, no. 3, pp. 250–303, 2003.
[13] J. Allison *et al.*, "Geant4 developments and applications," *IEEE Trans. Nucl. Sci.*, vol. 53, no. 1, pp. 270–278, Feb. 2006.
[14] M. Kuusela and V. M. Panaretos, "Statistical unfolding of elementary particle spectra: Empirical Bayes estimation and bias-corrected uncertainty quantification," *Ann. Appl. Stat.*, vol. 9, no. 3, pp. 1671–1705, Sep. 2015.
[15] D. Boor, *A Practical Guide to Splines*. New York, NY, USA: Springer-Verlag, 1978.
[16] R. Penrose, "A generalized inverse for matrices," *Math. Proc. Cambridge Philos. Soc.*, vol. 51, no. 3, pp. 406–413, Jul. 1955.
[17] A. N. Tikhonov and V. Y. Arsenin, *Solutions ILL-Posed Problems*. Washington, DC, USA: Winston, 1977.
[18] D. Calvetti, J. P. Kaipio, and E. Somersalo, "Aristotelian prior boundary conditions," *Int. J. Math. Comput. Sci.*, vol. 1, pp. 63–81, 2006.
[19] B. Efron and R. J. Tibshirani, *An Introduction to the Bootstrap*. London, U.K.: Macmillan, 1993.

[20] Barford and Davis, *Proc. Roy Soc. Lond. A, Math. Phys. Sci.*, vol. 214, p. 225, 1952.
[21] M. Conversi and P. Rothwell, "Angular distributions in cosmic ray stars at 3500 meters," *Il Nuovo Cimento*, vol. 12, no. 2, pp. 191–210, 1954.
[22] E. Heidbreder, K. Pinkau, C. Reppin, and V. Schönfelder, "Measurements of the distribution in energy and angle of high-energy neutrons in the lower atmosphere," *J. Geophys. Res.*, vol. 76, no. 13, pp. 2905–2916, 1971.
[23] S. Miyake, K. Hinotani, I. Katsumata, and T. Kaneko, "Cosmic ray nuclear interactions in nitrogen gas," *J. Phys. Soc. Jpn.*, vol. 12, no. 8, pp. 845–854, 1957.
[24] R. Saxena, "Ground-level atmospheric neutron flux measurements in the 10–170 MeV range," Ph.D. dissertation, Univ. New Hampshire, Durham, NH, USA, 1990.
[25] E. Lohrmann, "Angular distribution in cosmic ray stars," *Il Nuovo Cimento*, vol. 1, no. 6, pp. 1126–1140, 1955.
[26] M. R. Moser, J. M. Ryan, L. Desorgher, and E. O. Flückiger, "Atmospheric neutron measurements in the 10–170 MeV range," in *Proc. 29th Int. Cosmic Ray Conf.*, vol. 2. 2005, pp. 421–424.
[27] C. Hagmann, D. Lange, and D. Wright. *Monte Carlo Simulation of Proton-Induced Cosmic-Ray Cascades in the Atmosphere*, accessed on Jul. 2015. [Online]. Available: http://nuclear.llnl.gov/simulation/doc_cry_v1.7/cry_physics.pdf
[28] F. Ashton, H. J. Edwards, and G. N. Kelly, "The spectrum of cosmic ray neutrons at sea level in the range 0.4–1.2 GeV," *J. Phys. A, Gen. Phys.*, vol. 4, no. 3, p. 352, 1971.
[29] A. M. Preszler, G. M. Simnett, and R. S. White, "Angular distribution and altitude dependence of atmospheric neutrons from 10 to 100 MeV," *J. Geophys. Res.*, vol. 79, no. 1, pp. 17–22, 1974.